Electronic Supplementary Material (ESI) for Journal of Materials Chemistry A.

Supplementary Information

Multirole organics-induced scalable synthesis of MoS_2-monolayers/carbon mesoporous composite for high-performance lithium and potassium storage

Baorui Jia,[ab] Yongzhi Zhao,[a] Mingli Qin,*[ab] Wei Wang,*[cd] Zhiwei Liu,[a] Cheng-Yen Lao,[d] Qiyao Yu,[a] Ye Liu,[e] Haowang Wu,[a] Zili Zhang[a] and Xuanhui Qu[ab]

[a] Institute for Advanced Materials and Technology, University of Science and Technology Beijing, Beijing 100083, China.

[b] Beijing Key Laboratory for Advanced Powder Metallurgy and Particulate Materials, University of Science and Technology Beijing, Beijing 100083, China.

[c] Department of Materials Science and Engineering, College of Engineering, Peking University, Beijing 100871, China

[d] Department of Materials Science and Metallurgy, University of Cambridge, Cambridge CB3 0FS, UK.

[e] School of Material Science and Engineering, Xiangtan University, Hunan 411105, China.

Corresponding authors: qinml@mater.ustb.edu.cn (M. Qin); wwang_bj@126.com (W. Wang)

Experimental section

The synthesis of MoS_2 monolayers. All the reagents were used after purchase and without purification. In a typical procedure, 0.1 g ammonium molybdate tetrahydrate ($(NH_4)_6Mo_7O_{24}\bullet 4H_2O$) was dissolved into 5 mL water and 1.6 g oleylamine (OAm) was dissolved into 2 mL toluene. The two solutions were mixed ultrasoundly to produce milky white emulsion. Then 0.1 g sulfur (S) powder was added afterwards followed by 2 h of stirring. The mixture was then placed into a Teflon-lined stainless-steel autoclave. The autoclave was heated at 200 °C for 24 h in an oven and then cooled to room temperature naturally. The precipitate was washed with ethanol for several times and dried under ambient atmosphere. The obtained product was mesoporous composite of MoS_2 monolayers covered by an OAm organic coating (MoS_2/OAm). This organic-inorganic hybrid material can convert to the composite of MoS_2 monolayers embedded in carbon matrix (MoS_2/C) via an annealing process. MoS_2/OAm was calcined at 600 ^oC for 3 h under N_2 gas with a heating rate of 2 $^oC\cdot min^{-1}$ to form MoS_2/C.

Characterization. The compositions of the samples were studied by the X-Ray powder diffraction (XRD) using a Rigaku D/max-RB12 X-Ray diffractometer with Cu Kα radiation. The morphologies and compositions of the products were characterized by field emission scanning electron microscopy (SEM, JEOL, JSM-7001F). The transmission electron microscopy (TEM) images, high-resolution transmission electron microscopy (HRTEM) images and energy dispersive X-ray spectra (EDS) were obtained on a transmission electron microscopy (JEOL, JEM-2010). The Fourier transform infrared spectra (FT-IR) were recorded using a Nicolet 740 FT-IR spectrometer. Thermogravimetry (TG) analysis was performed with an STA-449F3 (NETZSCH-Gerätebau GmbH, Germany) at a heating rate of 20 $°C\cdot min^{-1}$ from 25 to 700 °C in air atmosphere. X-ray photoelectron spectra (XPS) were recorded with an ESCALAB 250 spectrometer (PerkinElmer) to characterize the surface composition. The Raman spectra were obtained on a microscopic confocal Raman spectrometer (Renishaw RM2000) using Ar^+ laser excitation with a wavelength of 514.5 nm. The surface area and pore-size distribution were measured by using a Belsorp-max surface area detecting instrument by N_2 physisorption at 77 K. Brunauer-Emmett-Teller (BET) surface areas were calculated using experimental points at a relative pressure of P/P_0=0.05-0.25. The pore size distributions were calculated by the Barrett-Joyner-Halenda (BJH) method.

Electrochemical property measurement. Electrochemical measurements were performed in the CR2023-type coin cells. The working electrode was fabricated by mixing the active materials (MoS_2/C) with acetylene black and a binder, poly(vinylidene fluoride), at weight ratio of 60:20:20. The mixture was dispersed in the N-methylpyrrolidone solvent to form slurry and uniformly pasted on the Cu foil with a blade. These prepared electrode sheets were dried at 120 ^oC in a vacuum oven for 12 h and pressed under a pressure of 200 kg m^{-2}. The CR2032-type coin cells were assembled in a glove box for electrochemical characterization. For LIBs, a non-aqueous solution of 1 M $LiPF_6$ in a 1:1 (v/v) mixture of ethylene carbonate (EC) and dimethyl carbonate (DMC) was used as the electrolyte, and the lithium metal worked as the reference electrode. The MoS_2/C loading was about 1 mg cm^{-2} without deducting the mass of carbon. The LIBs cells were galvanostatically charged and discharged in a current density of 100 $mA\cdot g^{-1}$ and 1000 $mA\cdot g^{-1}$ within a voltage range of 0.01-3 V using the LAND-CT2011A battery-testing instrument at room temperature. The cyclic voltammograms (CVs) were carried out on an electrochemistry workstation (CHI618D). Electrochemical impedance spectroscopy (EIS) was conducted at a frequency range of 0.1 Hz to 100 kHz. For KIBs, K foil was used as both the counter and reference electrodes, the electrolyte was a

0.8 M KPF_6 in a mixed solution of ethylene carbonate (EC) and diethyl carbonate (DEC) with a volume ratio of 1:1, and the glass fiber (GF/D) from Whatman was used as the separator. The galvanostatic charge and discharge process of KIBs was conducted within a voltage range of 0.01-2.5 V. The specific capacities of MoS_2/C for LIBs and KIBs were calculated based on the weight of MoS_2/C without deducing the mass of carbon.

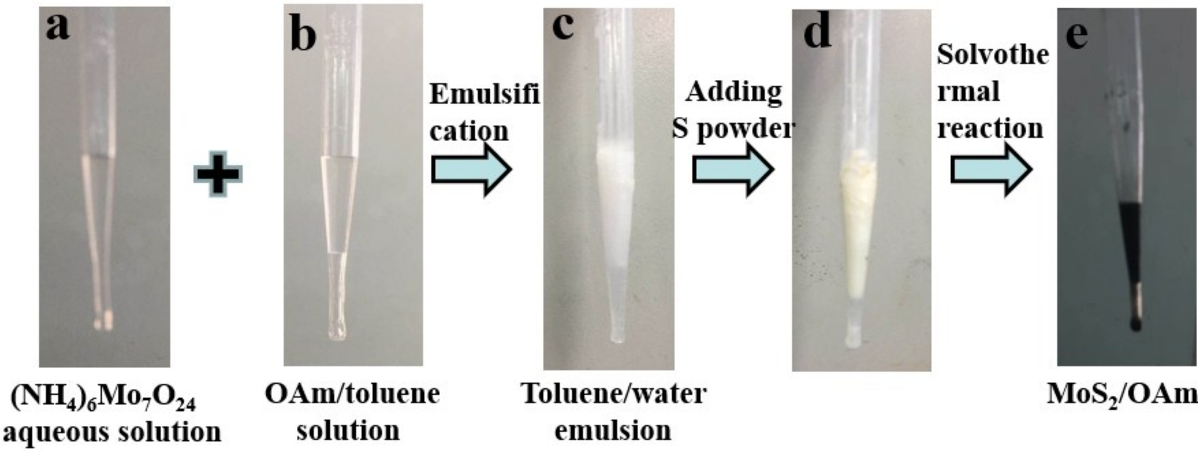

Fig. S1. The change of color during the synthesis of MoS_2/OAm.

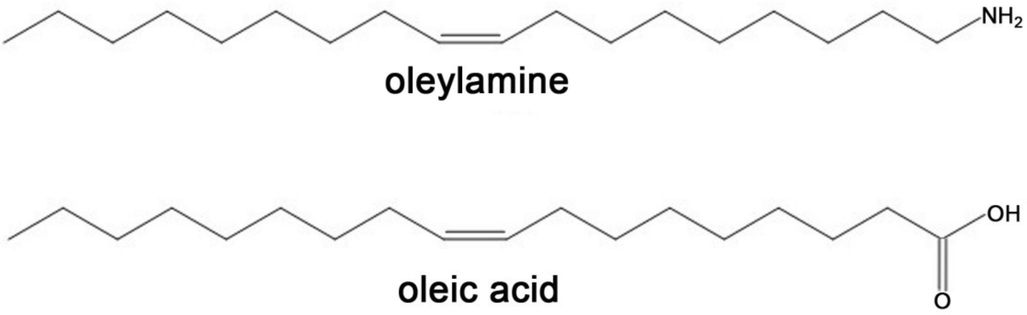

Fig. S2. The molecular structures of OAm and oleic acid. OAm exhibits basicity and affinity to metals through their NH_2 functional groups. The double bond ($C{=}C$) in the middle of the molecule is suggested to have coordination with metal atoms. OAm also facilitate scaling the synthetic reaction protocols because its cost is reasonably low.

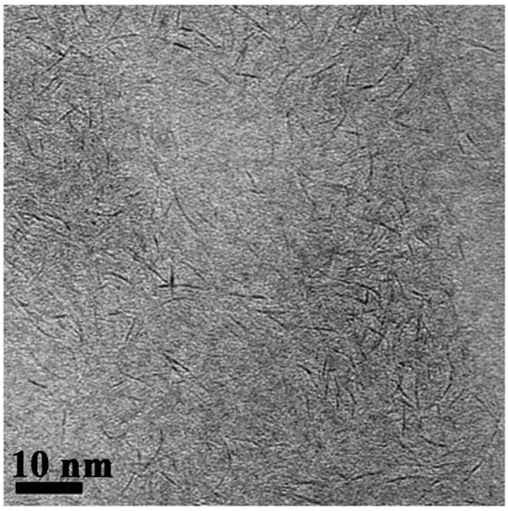

Fig. S3. TEM image of the MoS_2/OAm after washing by cyclohexane and methylbenzen. The product presents a similar morphology compared to the sample before washing, and the MoS_2 monolayers are still randomly dispersed in OAm matrix.

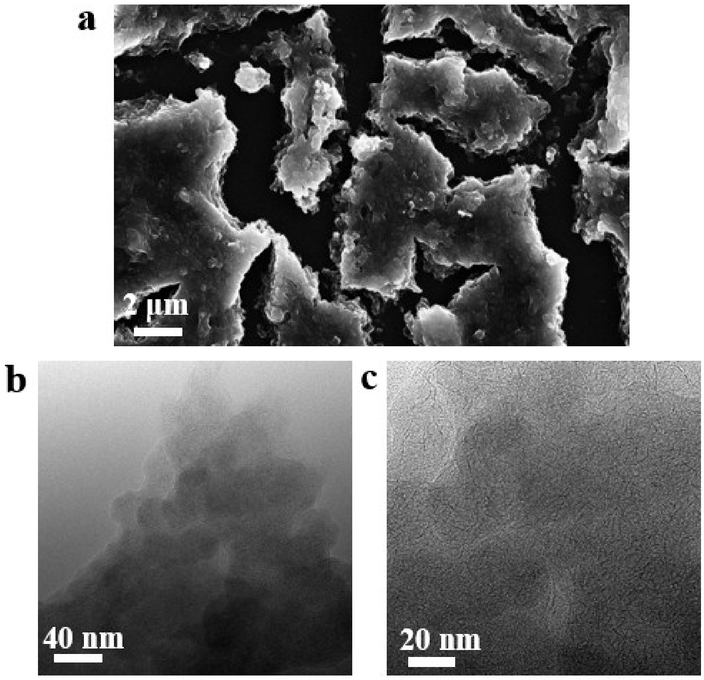

Fig. S4. (a) SEM image and (b, c) TEM images of the solvothermal product prepared without addition of toluene. Because soft template emulsion is absent, the product is dense and does not have pores.

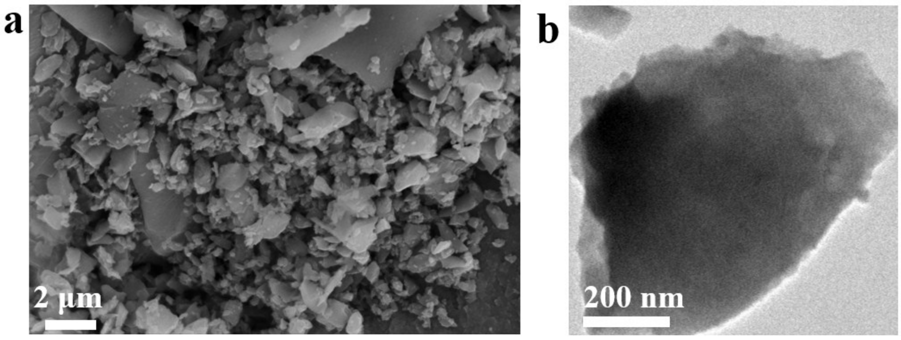

Fig. S5. (a) SEM image and (b) TEM image of the annealed product prepared without addition of toluene. After annealing, aggregation becomes much more apparent, and the products are very dense micro-sized particles.

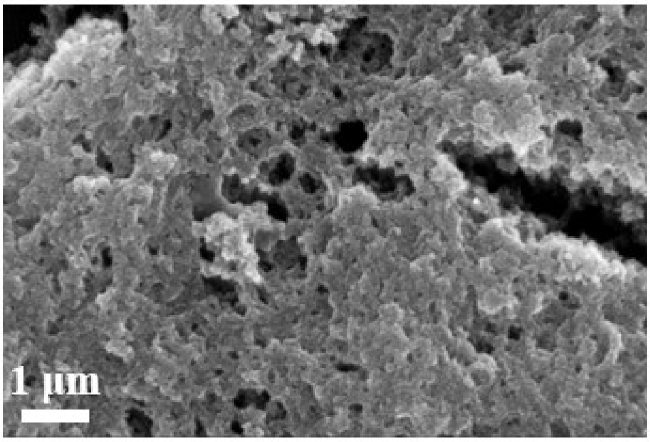

Fig. S6. SEM image of the mesoporous MoS_2/OAm composite, demonstrating the existence of pores.

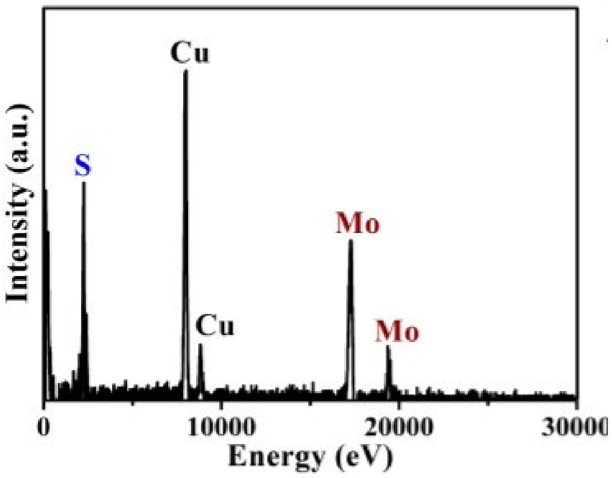

Fig. S7. EDS spectra of MoS_2/OAm mesoporous composites

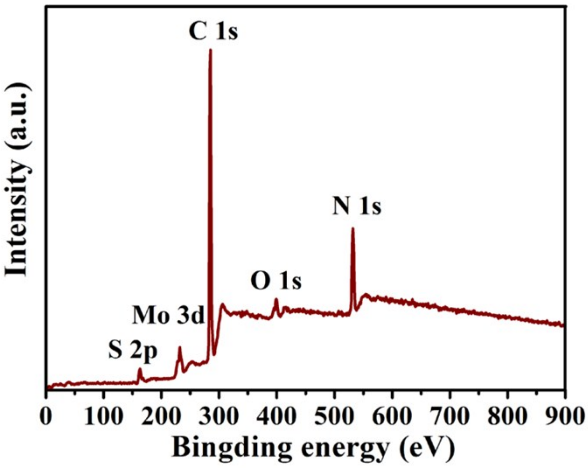

Fig. S8. XPS spectra of MoS_2/OAm. The peaks from Mo, S, C, O and N are observed, indicating the formation of the molybdenum sulfide and OAm composite.

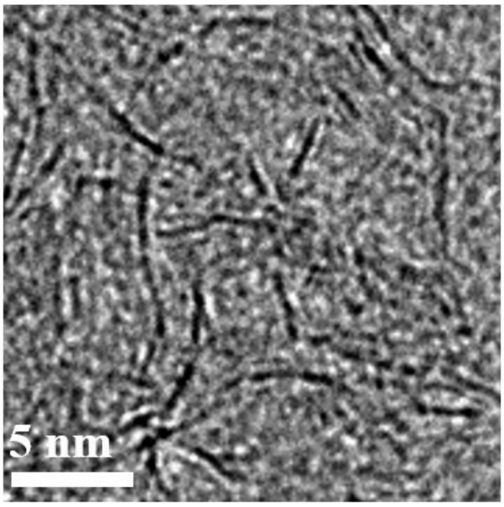

Fig. S9. TEM image of MoS_2/C shows that the MoS_2 monolayers were disorderly dispersed in the carbon matrix.

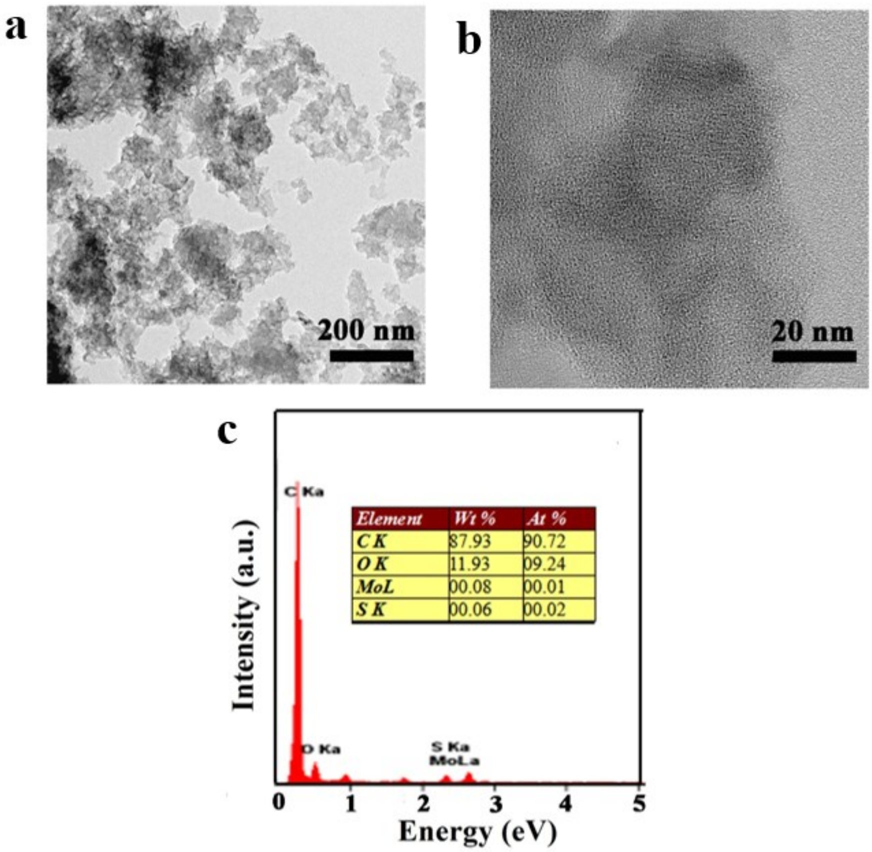

Element	Wt %	At %
C K	87.93	90.72
O K	11.93	09.24
MoL	00.08	00.01
S K	00.06	00.02

Fig. S10. (a, b) TEM images and (c) EDS spectra of MoS_2/C after treatment in nitric acid solution. In TEM images, no MoS_2 layers can be observed. The EDS result also reveals that MoS_2 has been dissolved. The lattice and layers of graphite are not found, confirming its amorphous nature of C in MoS_2/C.

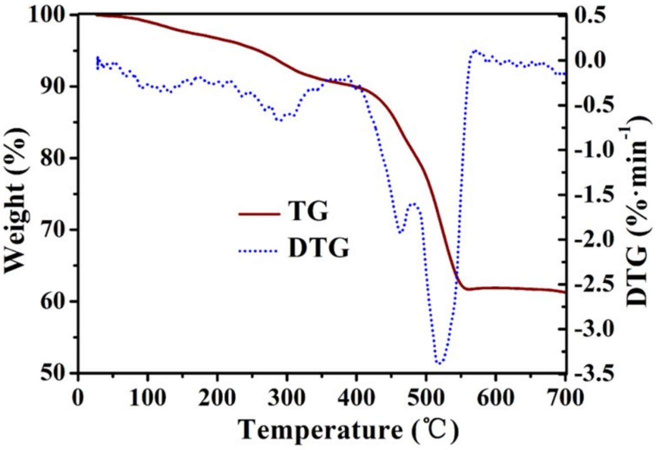

Fig. S11. TG/DTG spectra in air of MoS_2/C.

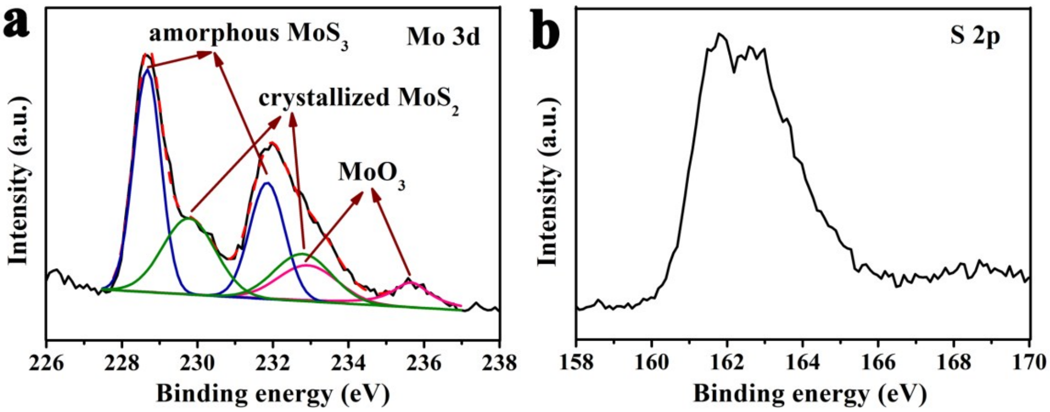

Fig. S12. (a) XPS Mo 3d spectra and (b) XPS S 2p spectra of MoS_2/OAm.

Three doublets of Mo $3d_{5/2}$ and Mo $3d_{3/2}$ are obtained after fitting the Mo 3d pattern of MoS_2/OAm. The doublet of Mo $3d_{5/2}$ and Mo $3d_{3/2}$ peaks at the binding energy ~ 228.7 and 231.9 eV is indexed to Mo^{4+} oxidation station of amorphous MoS_3. The doublet at the binding energy ~ 229.8 and 232.8 eV is indexed to Mo^{4+} of crystallined 2H-MoS_2. Note that the Mo binding energies in amorphous MoS_3 and crystallized MoS_2 are different as reported in previous researches, although their Mo elements have same 4^+ valence state. The molar ratio of crystalline MoS_2 phase and amorphous MoS_3 phase is about 2:3 according to their peak area ratio. However, because XPS is a surface measurement technique, the content of amorphous MoS_3 in the whole sample cannot be determined.

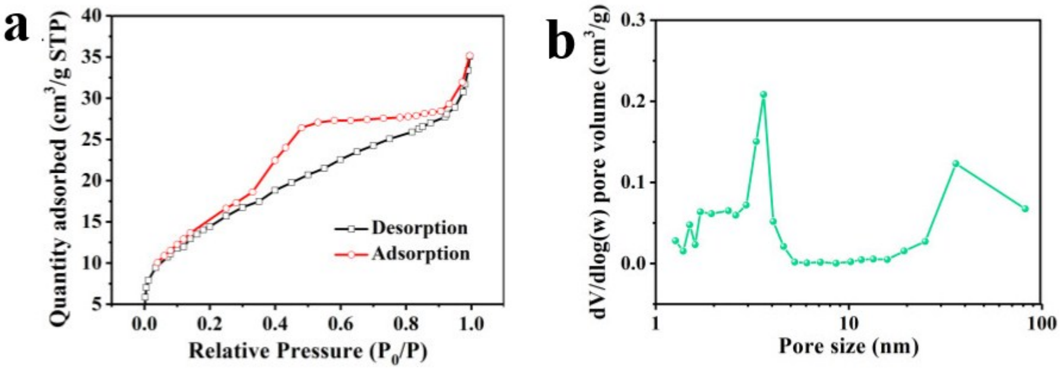

Fig. S13. (a) N_2 adsorption-desorption isotherms, and (b) BJH pore size distribution curve of MoS_2/C.

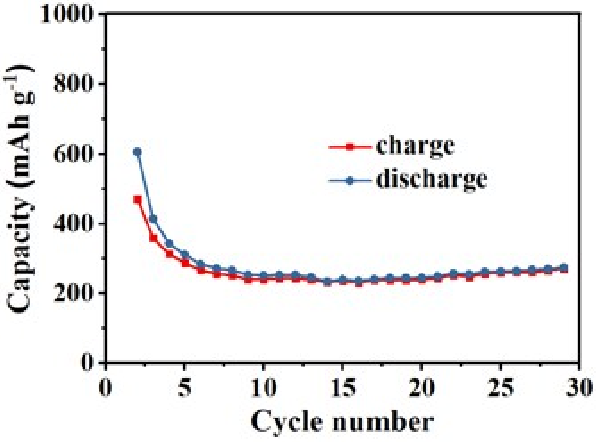

Fig. S14. Cycling performance at 100 mA·g^{-1} of the carbon material prepared from MoS_2/C by removing MoS_2 with acid washing. The specific capacity of the carbon is about 270 mAh·g^{-1}.

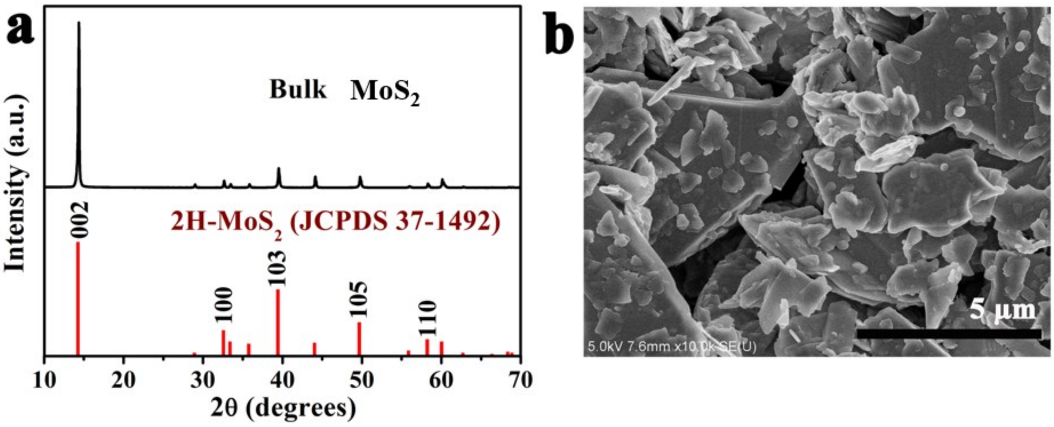

Fig. S15. (a) XRD pattern and (b) SEM image of MoS$_2$ bulk material.

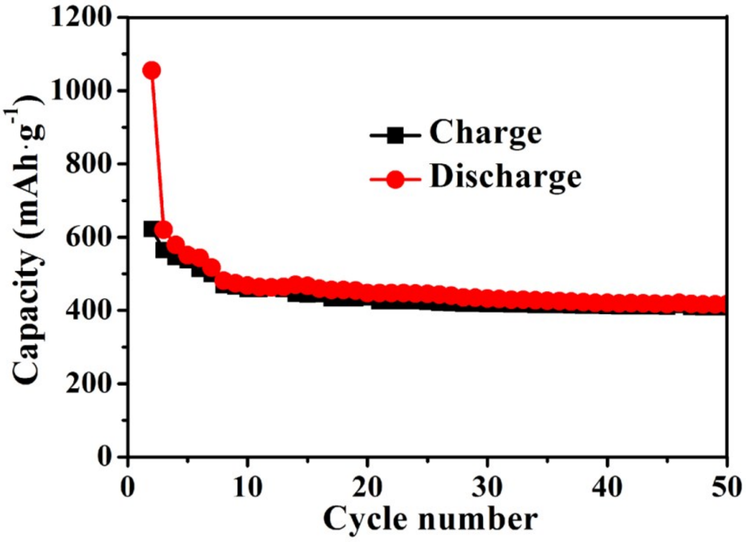

Fig. S16. Cycling performances of bulk MoS_2 material at a density of 100 mA·g^{-1}.

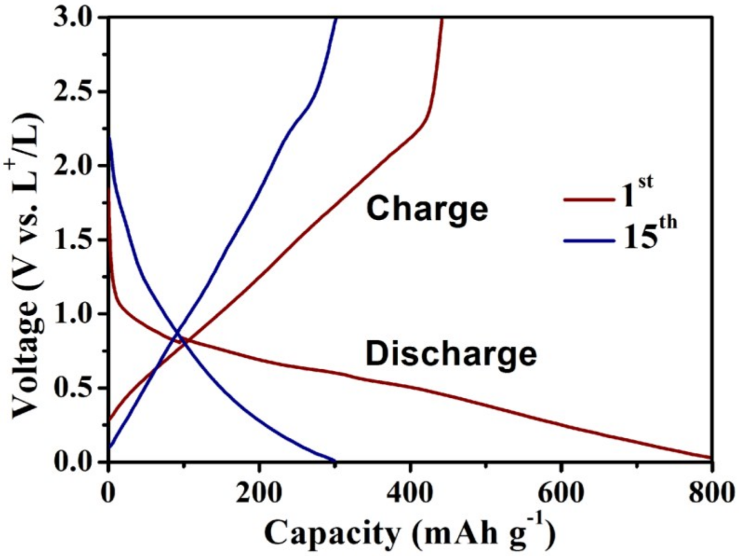

Fig. S17. The discharge/charge profiles of MoS_2 bulk material at a density of 1000 mA·g^{-1}.

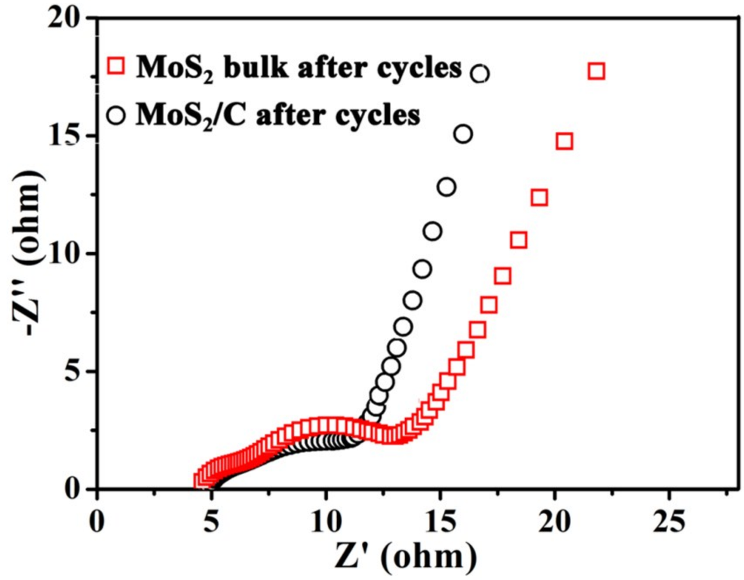

Fig. S18. Nyquist plots of MoS_2/C and bulk MoS_2 material after cycles. Compared with the sample before cycles, the diameter of semicircles is significantly decreased after cycling, which is in accordance with the activation process.

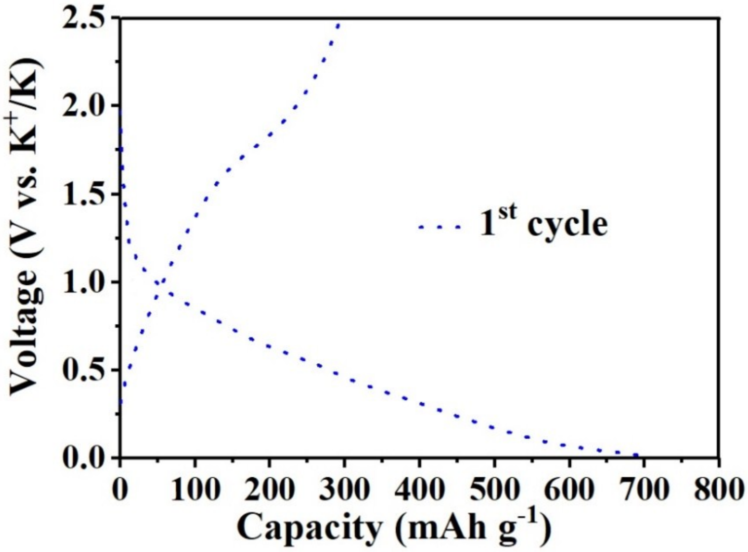

Fig. S19. The discharge/charge profiles of MoS_2/C at the first cycle at a density of 500 mA·g^{-1}

Table S1 The performances of the reported excellent MoS_2 and our MoS_2 monolayers/C LIB anodes.

MoS_2-based anode materials	Capacity retention	Reference
MoS_2-Coated Three-Dimensional Graphene	877 and 665 mAh·g^{-1} after 50 cycles at 100 and 500 mA·g^{-1}	[1]
Few-Layer MoS_2 Anchored on Carbon Nanosheet	709 mAh·g^{-1} after 520 cycles at 2000 mA·g^{-1}	[2]
2D MoS_2 Nanowall	880 mAh·g^{-1} after 50 cycles at 100 mA·g^{-1}	[3]
MoS_2 Nanoflakes Encapsulated in Carbon Nanofibers	350 mAh·g^{-1} at 1000 mA·g^{-1}	[4]
Quasi-Hollow MoS_2 Microspheres Encapsulated Porous Carbon	670 mAh·g^{-1} after 100 cycles at 1000 mA·g^{-1}	[5]
Reduced Graphene Oxide/MoS_2 Nanoflowers	680 mAh·g^{-1} after 250 cycles at 500 mA·g^{-1}	[6]
MoS_2 Nanosheets Hosted in Mesoporous Carbon Nanofibers	950 mAh·g^{-1} after 100 cycles at 100 mA·g^{-1}	[7]
Hierarchical MoS_2 Tubular Structures Internally Wired by Carbon Nanotubes	1100 mAh·g^{-1} after 200 cycles at 500 mA·g^{-1}	[8]
Ultrathin MoS_2/Nitrogen-Doped Graphene Nanosheets	850 mAh·g^{-1} after 50 cycles at 1000 mA·g^{-1}	[9]
Single-Layered Ultrasmall Nanoplates of MoS_2 Embedded in Carbon Nanofibers	1007 mAh·g^{-1} after 100 cycles at 1000·mA g^{-1}	[10]
MoS_2 Nanosheets Vertically Grown on Graphene Sheets	1077 mAh·g^{-1} after 150 cycles at 100·mA g^{-1}	[11]
Few-Layered MoS_2 with S-Doped Graphene	1672 mAh·g^{-1} at 100 mA·g^{-1}	[12]
Carbon-Sandwiched Monolayered MoS_2	807 mAh·g^{-1} after 100 cycles at 100 mA·g^{-1}	[13]
MoS_2 Nanosheets Supported on N-doped Carbon Nanoboxes	952 mAh·g^{-1} after 200 cycles at 400 mA·g^{-1}	[14]
Highly Oriented Configuration by Few-Layer MoS_2	1009.2 mAh·g^{-1} after 500 cycles at 500 mA·g^{-1}	[15]
MoS_2 Monolayers Embedded in Carbon Matrix	1001 mAh·g^{-1} after 50 cycles at 100·mA g^{-1}; 663 mAh·g^{-1} after 500 cycles at 1000 mA·g^{-1}	[this work]

Table S2 The performance comparison of some reported anodes and our MoS_2 monolayers/C anodes for KIBs.

Materials	**Capacity retention**	**Reference**
Hard Carbon	216 $mAh{\cdot}g^{-1}$ after 100 cycles at 27.9 $mA{\cdot}g^{-1}$	[16]
M-KTO	78 $mAh{\cdot}g^{-1}$ after 100 cycles at 50 $mA{\cdot}g^{-1}$	[17]
Sn_4P_3/C	307.2 $mAh{\cdot}g^{-1}$ after 50 cycles at 50 $mA{\cdot}g^{-1}$	[18]
Graphite	100 $mAh{\cdot}g^{-1}$ after 50 cycles at 140 $mA{\cdot}g^{-1}$	[19]
MoS_2	65 $mAh{\cdot}g^{-1}$ after 200 cycles at 20 $mA{\cdot}g^{-1}$	[20]
Sn-C Composite	110 $mAh{\cdot}g^{-1}$ after 30 cycles at 25 $mA{\cdot}g^{-1}$	[21]
Nitrogen-Doped Graphene	210 $mAh{\cdot}g^{-1}$ after 100 cycles at 100 $mA{\cdot}g^{-1}$	[22]
Black Phosphorus	120 mAh g^{-1} at 500 $mA{\cdot}g^{-1}$	[23]
Activated carbon	100 $mAh{\cdot}g^{-1}$ after 100 cycles at 200 $mA{\cdot}g^{-1}$	[24]
MoS_2 Monolayers Embedded in Carbon Matrix	180 $mAh{\cdot}g^{-1}$ after 240 cycles at 500·mA g^{-1}; 391 $mAh{\cdot}g^{-1}$ at 50 $mA{\cdot}g^{-1}$ after 35 rate cycles	[this work]

References

[1] X. Cao, Y. Shi, W. Shi, X. Rui, Q. Yan, J. Kong, H. Zhang, *Small* **2013**, 9, 3433.

[2] J. Zhou, J. Qin, X. Zhang, C. Shi, E. Liu, J. Li, N. Zhao, C. He, *ACS nano* **2015**, 9, 3837.

[3] U. K. Sen, S. Mitra, *ACS Appl. Mater. Inter.* **2013**, 5, 1240.

[4] C. Zhao, J. Kong, X. Yao, X. Tang, Y. Dong, S. L. Phua, X. Lu, *ACS Appl. Mater. Inter.* **2014**, 6, 6392.

[5] Z. Wan, J. Shao, J. Yun, H. Zheng, T. Gao, M. Shen, Q. Qu, H. Zheng, *Small* **2014**, 10, 4975.

[6] F. Xiong, Z. Cai, L. Qu, P. Zhang, Z. Yuan, O. K. Asare, W. Xu, C. Lin, L. Mai, *ACS Appl. Mater. Inter.* **2015**, 7, 12625.

[7] J. Kong, C. Zhao, Y. Wei, X. Lu, *ACS Appl. Mater. Inter.* **2015**, 7, 24279.

[8] Y. M. Chen, X. Y. Yu, Z. Li, U. Paik, X. W. D. Lou, *Sci. Adv.* **2016**, 2, e1600021.

[9] K. Chang, D. Geng, X. Li, J. Yang, Y. Tang, M. Cai, R. Li, X. Sun, *Adv. Energy Mater.* **2013**, 3, 839.

[10] C. Zhu, X. Mu, P. A. Van Aken, Y. Yu, J. Maier, *Angew. Chem. Int. Ed.* **2014**, 53, 2152.

[11] Y. Teng, H. Zhao, Z. Zhang, Z. Li, Q. Xia, Y. Zhang, L. Zhao, X. Du, Z. Du, P. Lv, *ACS Nano* **2016**, 10, 8526.

[12] X. Wang, G. Li, M. H. Seo, F. M. Hassan, M. A. Hoque, Z. Chen, *Adv. Energy Mater.* **2015**, 5.

[13] J. Shao, Q. Qu, Z. Wan, T. Gao, Z. Zuo, H. Zheng, *ACS Appl. Mater. Inter.* **2015**, 7, 22927.

[14] X. Y. Yu, H. Hu, Y. Wang, H. Chen, X. W. D. Lou, *Angew. Chem. Int. Ed.* **2015**, 54, 7395.

[15] S. Zhang, B. Chowdari, Z. Wen, J. Jin, J. Yang, *ACS Nano* **2015**, 9, 12464.

[16] Z. Jian, Z. Xing, C. Bommier, Z. Li, X. Ji, *Adv. Energy Mater.* **2016**, 6, 1501874.

[17] Y. Dong, Z. Wu, S. Zheng, X. Wang, J. Qin, S. Wang, X. Shi, X. Bao, *ACS Nano* **2017**, 11, 4792.

[18] W. Zhang, J. Mao, S. Li, Z. Chen, Z. Guo, *J. Am. Chem. Soc.* **2017**, 139, 3316.

[19]Z. Jian, W. Luo, X. Ji, *J. Am. Chem. Soc.* **2015**, 137, 11566.

[20]X. Ren, Q. Zhao, W. D. McCulloch, Y. Wu, *Nano Research* **2017**, 10(4), 1313.

[21] I. Sultana, T. Ramireddy, M. M. Rahman, Y. Chen, A. M. Glushenkov, *Chem. Commun.* **2016**, 52, 9279.

[22] K. Share, A. P. Cohn, R. Carter, B. Rogers, C. L. Pint, *ACS Nano* **2016**, 10, 9738.

[23] I. Sultana, T. Ramireddy, M. M. Rahman, Y. Chen, A. M. Glushenkov, *J. Mater. Chem. A* **2017**, 5, 23506.

[24] Z. Tai, Q. Zhang, Y. Liu, H. Liu, S. Dou, *Carbon* **2017**, 123, 54.